# Enhanced Design of Airborne Radiation Sensor for Improved Survivability During Deployment Impact

Pengcheng Yin, *Associate Member, IEEE*, Jonghwan Ha, Junbo Yang, *Student Member, IEEE*, Karthik Deo, Yangyang Lai, *Member, IEEE*, and Seungbae Park, *Fellow, IEEE*

***Abstract*—By employing optimized outer packaging designs and materials, the impact energy can be effectively absorbed or dissipated, thereby preventing potential damage to interconnections and chips. This includes mitigating solder-joint fractures, chip cracks, pad cratering or lifting, and other mechanical stresses that commonly result from impact forces. To ensure that the internal ionic sensor remains resilient to moisture intrusion and can endure impact velocities of up to 30 mph, advanced packaging solutions have been developed. In this study, the ANSYS/LS-DYNA finite element analysis (FEAs) tool was utilized to evaluate the performance of various packaging designs in minimizing the shock energy transferred to the printed circuit board (PCB). Modifications were made to the external foam packaging to increase the effective thickness and stiffness of the PCB, thus limiting its deformation under impact. These adjustments involved testing several configurations, including a two-layer foam system, a single-layer foam, and variations in the foam material's stress-strain characteristics. The results demonstrated a significant reduction in PCB deformation—by 86.9%—with the final design achieving a deformation of just 52 $\mu$m, compared to 398.7 $\mu$m in the initial design. Furthermore, the simulations of the final design were conducted for different drop orientations to ensure that out-of-plane deformations remained within the same order of magnitude, regardless of the drop direction.**

***Index Terms*—Airborne package, drop test simulation, foam packaging, high-speed drop impact.**

## I. Introduction

As CONSUMER demand for electronic products continues to surge, ensuring product reliability during transportation has become a critical priority. The outer packaging plays a pivotal role in protecting devices from damage caused by mechanical stresses, such as bumps, drops, and vibrations during shipping. To address these challenges, significant research has focused on enhancing packaging reliability through advancements in both thermal management and shock absorption. For instance, Ahmed et al. [1] investigated large package reflow processes to prevent solder bridging and improve solder quality, ultimately increasing the fatigue life of large packages. Lai et al. [2], [3], [4], [5], [6] leveraged machine learning to optimize reflow profiles for various package sizes assembled on printed circuit boards (PCBs), ensuring consistent solder quality and potentially improving the fatigue life of the package assembly. Similarly, Ha et al. [7], [8], [9] explored the influence of solder shape and volume on the fatigue life of electronic packages. These studies highlight the critical role of solder joint integrity in package reliability, particularly in harsh environments. Designing shock-resistant packaging and incorporating shock-absorbent materials are essential to minimize the transfer of impact energy to sensitive components, such as solder joints, which are especially vulnerable during shipping. Oh et al. [10] utilized a design of experiments (DOEs) approach to enhance the shock resistance of cartridge containers by optimizing anti-shock structures. Pan and Chen [11] improved the shock-proof capabilities of electronic displays by optimizing the fastening system, adding spring washers, and increasing the thickness of the top plastic casing. Foam, a well-known shock-absorbing material, is widely used in applications, such as motorcycle helmets [12] and vehicle safety systems [13], to protect individuals in the event of collisions. Numerical simulations, particularly finite element analysis (FEAs), are invaluable for studying the dynamic responses of packaging systems to impact events, which often involve short-duration transients and nonlinear behavior. ANSYS/LS-DYNA, a well-established tool for such analyses, is capable of accurately simulating high-frequency responses, large deformations, complex contact scenarios, and material failures. In this study, ANSYS/LS-DYNA was employed to model high-speed impacts, utilizing its comprehensive library of foam models tailored to different materials. These models demonstrated high fidelity in replicating real-world conditions, yielding reliable simulation outcomes [14], [15], [16], [17], [18], [19]. Previous research has validated the accuracy of LS-DYNA's low-density foam material model in predicting critical metrics, such as peak deceleration, stress distribution, and deformation during impact [20]. Sambamoorthy and Halder [21] compared four distinct LS-DYNA foam models—low-density foam, crushable foam, Bilkhu-Dubois foam, and Fu-Chang foam—against experimental data for polyurethane foam, achieving results that closely aligned with real-world performance.

In this study, outer packaging has been developed, and internal mechanical structure was optimized for the airborne ionic sensor that is expected to be deployed from the air with 30-mph impact velocity. A prior study [22] conducted a parametric analysis that offered preliminary insights into packaging design, demonstrating that two-layer foam systems provide

Received 29 September 2024; revised 2 March 2025; accepted 12 April 2025. Date of publication 22 April 2025; date of current version 8 July 2025. Recommended for publication by Associate Editor C. Bailey upon evaluation of reviewers' comments. *(Corresponding author: Pengcheng Yin.)*

The authors are with the Department of Mechanical Engineering, The State University of New York at Binghamton, Binghamton, NY 13902 USA (e-mail: pyin2@binghamton.edu).

Digital Object Identifier 10.1109/TCPMT.2025.3563253

TABLE I
SELECTED FOAM MECHANICAL PROPERTIES

| **Material** | **Properties** | |
|---|---|---|
| | ***Young's Modulus (MPa)*** | ***Density (kg/m$^3$)*** |
| EV50 | 0.38 | 48 |
| BDJN300 | 0.46 | 50 |

superior shock resistance compared to single-layer configurations. Additionally, a textured "pinball" surface was found to outperform plain surfaces in terms of shock absorption. Building on this earlier work, the current study revisits the outer packaging design and foam material properties to reflect updates in the core product design. To further improve the shock performance and refine material selection guidelines, the stress-strain curves of foam samples were manually adjusted to evaluate the impact of different foam properties on overall packaging performance and include the stiffener rib design and PCB thickness parameter to enhance the integrity of entire packaging.

## II. Simulation and Validation of Foam Model

### A. Foam Sample Characterization

Two closed-cell foam samples were provided from the vendor, the so-called EV50 and BDJN300. The foams shown in Table I are the test sample for material characterization and the Young modulus and density are measured.

To validate the finite element model of foam, the stress-strain curve as input parameters should be obtained from the compression experiment. The experimental setup and stress-strain curves are shown in Fig. 1.

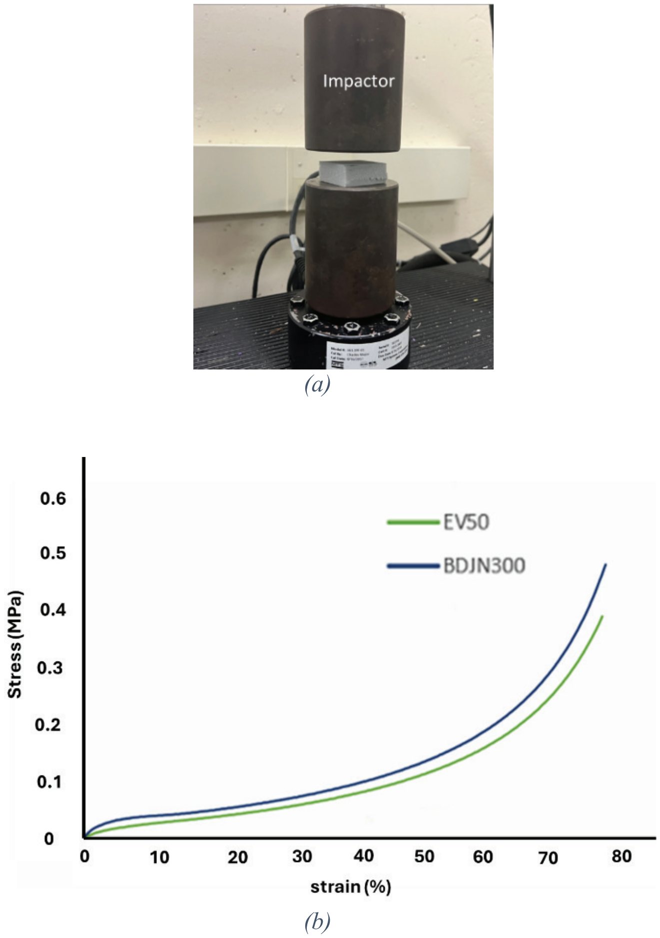


Fig. 1. Experimental setup and compression results for foam samples. (a) Compression experiment instrument. (b) Stress-strain property for EV50 and BDJN300.

### B. Foam Model Validation

The finite element method (FEM) was employed to accurately obtain the stress-strain curve for a 30-mph impact, as it is a straightforward and highly effective approach for this type of analysis. The first step involved validating the foam model to ensure accurate stress-strain curve predictions for further use. The setup for the compression simulation constrained all degrees of freedom (DOF) on the foam model's bottom surface (Fig. 2) and applied a displacement to the top surface, replicating the conditions observed in the physical compression experiment.

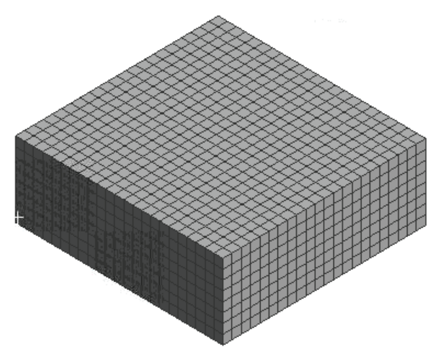

Fig. 2. Finite element model of foam.

In ANSYS/LS-DYNA, one of the key input parameters required for these simulations is the foam's stress-strain data. The force-versus-displacement curve obtained from the simulation was compared with the experimental data to verify the accuracy of the foam model. Fig. 3 presents the comparison results for each foam type. The simulations demonstrated a strong correlation with the experimental results for all foam samples. Consequently, all foam models used in the analysis have been successfully validated.

### C. Foam Property Prediction

Following the validation of the finite element model for each foam, prediction simulations were performed to obtain the stress-strain curves under a 30-mph impact. The primary reason for conducting these prediction simulations is that the foam's strain rate continuously changes during the impact, as the acceleration varies throughout the event. To accurately replicate the full impact scenario, two rigid plates were applied at the top and bottom of the foam model, as shown in Fig. 4(a). A 30-mph impact velocity was applied to the top rigid plate (impactor), while the bottom rigid plate was fixed, simulating a grounded surface in the prediction simulation. The predicted stress-strain curves for each foam under the 30-mph impact

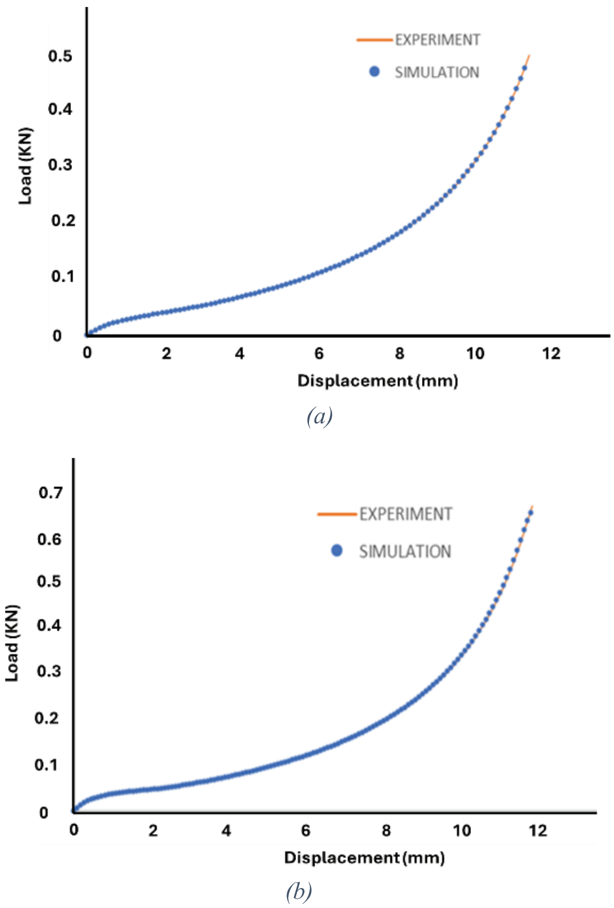


Fig. 3. Load-displacement result between simulation and experiment. (a) EV50. (b) BDJN300.

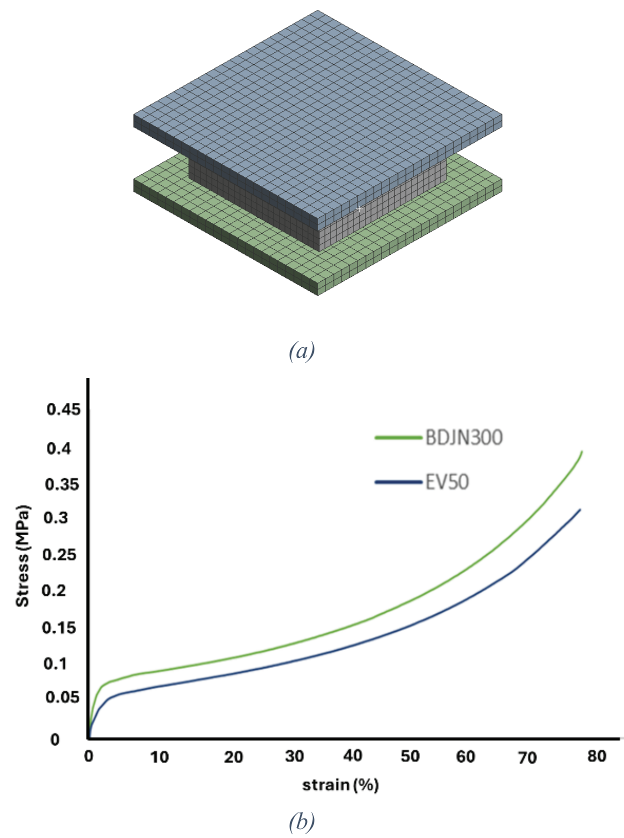


Fig. 4. Prediction FEA foam model and simulation results. (a) Prediction FEA Foam model. (b) Predicted stress-strain property for foam sample.

velocity are presented in Fig. 4(b). These simulations provide insight into how each foam material behaves under dynamic impact conditions, reflecting their real-world performance during high-speed impacts.

## III. High-Speed Drop Impact Simulation

### A. Simulation Setting of High-Speed Drop Impact

In this study, the design of the internal components without outer packaging is illustrated in Fig. 5. The internal assembly consists of a battery holder, four coin-cell batteries, a chamber housing the central electrode, a PCB, and a bottom stiffener. In order to save the computational time, the small components were eliminated, such as capacitors and resistors. Because those components could not impact the PCB behavior during impact. Several structural elements can be optimized to minimize PCB deformation, including the thickness of the PCB, the design of the bottom stiffener, the material selection of outer packaging, and the integration of the outer packaging.

The basic setup for the drop impact simulation in ANSYS/LS-DYNA involves an impact velocity of 30 mph, with the impact target modeled as marble to represent a worst case scenario. A tetrahedral mesh was applied to the foam outer packaging, as this mesh type is well-suited for handling the high distortion deformations that occur in the foam during the impact event.

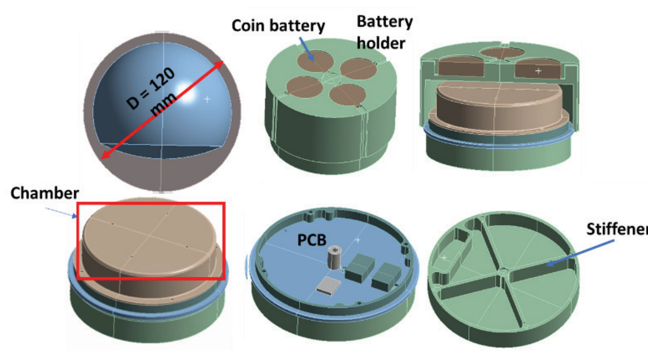


Fig. 5. Detailed structure of simulation model.

### B. Simulation Result of Initial Design

In previous work [22], various structures, shapes, and textures of foam packaging were studied. The results indicated that a double-layer design, consisting of a soft outer layer and a hard inner layer, outperformed the single-layer design for outer foam packaging. Additionally, the stress-strain curve for each foam was magnified fivefold compared to the originally measured curve (a detailed analysis of the effects of different stress-strain curves is provided in Section III-D). Based on these findings, the initial design adopted the double-layer configuration. The simulation results for maximum out-of-plane deformation of PCB are presented in Fig. 6. The

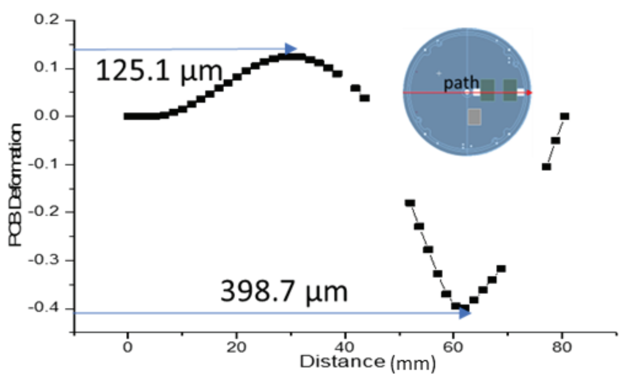


Fig. 6. Maximum out-of-plane deformation along the path of initial design.

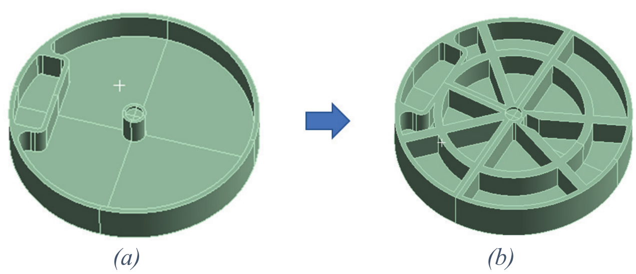


Fig. 7. 3-D model of bottom stiffener design. (a) No rib. (b) Stiffener ribs in different directions.

location and magnitude of the maximum deformation are easily identifiable—occurring between the two cutoff areas—with a value of approximately 400 $\mu$m, which significantly exceeds the target limit of 100 $\mu$m. Consequently, multiple comparative simulations were conducted to reduce the PCB deformation and optimize the weight of the entire device.

### C. Effect of Bottom Stiffener and PCB Thickness

The bottom stiffener enhances the overall structural integrity/stiffness of the model and, along with increasing PCB thickness, helps to minimize PCB deformation. As shown in Fig. 7(b), stiffener ribs were strategically designed and oriented in different directions to reduce the shock-induced deformation of the PCB, since the stiffener ribs attached to the bottom side of PCB could increase the effective stiffness of PCB to further reduce the deformation of PCB. This design approach not only decreases the rib density but also significantly reduces the weight of the bottom stiffener. Regarding PCB thickness, three cases were evaluated: 65, 93, and 125 mils. Each thickness was analyzed to determine its effectiveness in minimizing deformation while balancing structural integrity and weight considerations.

As shown in Fig. 8 and Table II, the results indicate several key findings. First, increasing the PCB thickness leads to a significant reduction in deformation, with the 125-mil PCB showing the least deformation among the cases studied. Second, the inclusion of stiffener ribs has a substantial impact on reducing PCB deformation, particularly in the case of the 65-mil PCB, where the deformation was reduced by 85%. Third, the difference in deformation between the three PCB thicknesses becomes minimal when stiffener ribs are incorporated, further underscoring the importance of the stiffener ribs in providing strong structural support during impact.

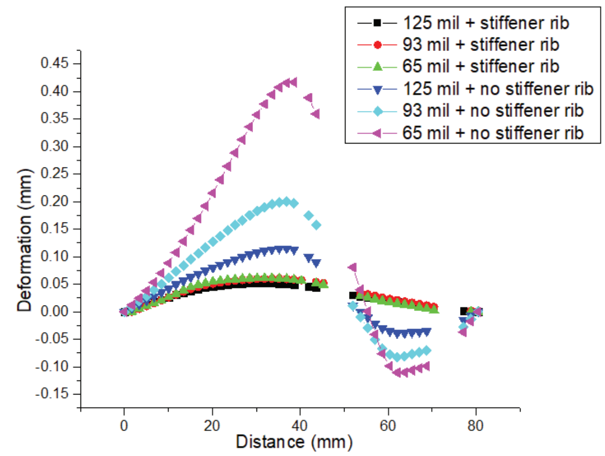


Fig. 8. Maximum out-of-plane deformation of PCB along the central of PCB in different design cases.

TABLE II
SIMULATION RESULTS OF THE STUDY EFFECT OF STIFFENER RIB DESIGN

| PCB Deformation | | |
|---|---|---|
| PCB Thickness | Stiffener Rib | No stiffener Rib |
| 65 mil | 62 µm | 417 µm |
| 93 mil | 60 µm | 200 µm |
| 125 mil | 52 µm | 114 µm |

### D. Effect of Material Property and Structure of Foam Packaging

In the simulation, the stress-strain curve of the foam serves as a critical input parameter. To investigate the effect of different stress-strain behaviors, the curves were systematically adjusted, as illustrated in Fig. 9. The figure shows that the stress-strain data for the hard foam were magnified by factors of 2, 3, 4, and 6, while for the soft foam, the data were magnified by factors of 3, 4, and 5, based on the original stress-strain data. Referring back to the previous study citebib:23, the double-layer foam packaging structure was initially selected due to its superior performance. However, since modifications have been made to the design of the internal components, the structure of the foam packaging must be re-evaluated to ensure optimal performance under the new conditions.

The results are presented in Fig. 10. On the $x$-axis, different combinations of stress-strain curves for soft and hard foam materials are displayed. The most notable observation is that the combination of the original EV50 and BDJN300 foam materials results in the largest PCB deformation, approximately 631 $\mu$m. In contrast, for the magnified cases, the PCB deformation consistently remains around 60 $\mu$m, even with a monotonic layer design. According to the properties of foam materials, the area enclosed by the stress-strain curve represents the energy absorbed by the foam material.

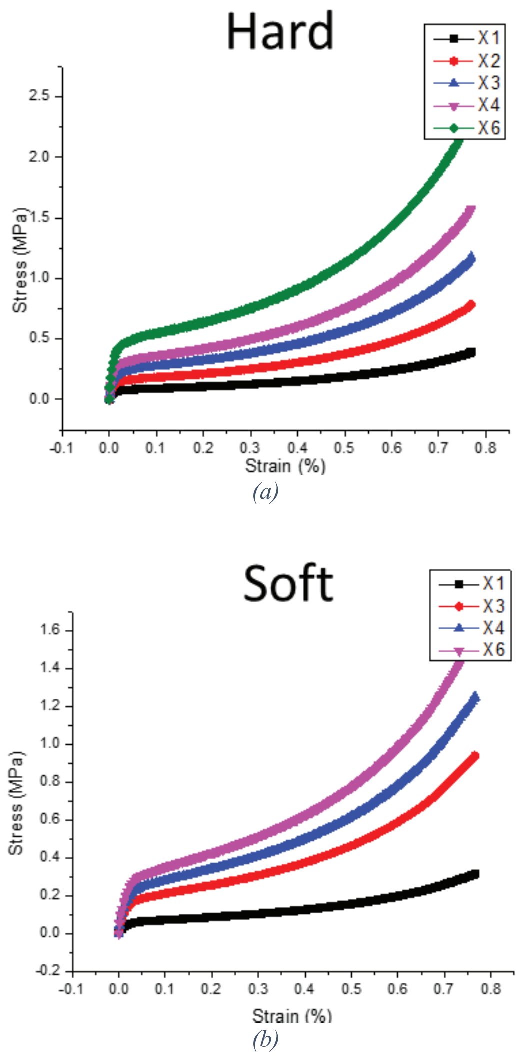


Fig. 9. Stress-strain curves for hard and soft foam material. (a) Stress-strain data for hard foam material. (b) Stress-strain data for soft foam material.

This indicates that higher stress-strain curves correspond to greater energy absorption. Consequently, foam materials with higher stress-strain curves are expected to result in lower PCB deformation. Based on these findings, the monotonic layer design was selected for the foam packaging in subsequent simulations. Furthermore, the simulation results suggest that a wide range of foam materials can be effectively used in this application.

## *E. Effect of Texture and Volume of Foam Packaging*

As the design of the internal components and the foam's stress-strain curve was modified, the texture and volume of the foam packaging also needed to be re-evaluated based on previous studies [22]. In earlier research, the outer pimple texture demonstrated superior shock absorption performance compared to the bare texture. However, the pimple structure significantly increases the volume of the packaging. To determine if the outer texture is essential, the comparison simulations were conducted using a bare outer texture. The FEA models used in the impact simulation are shown in

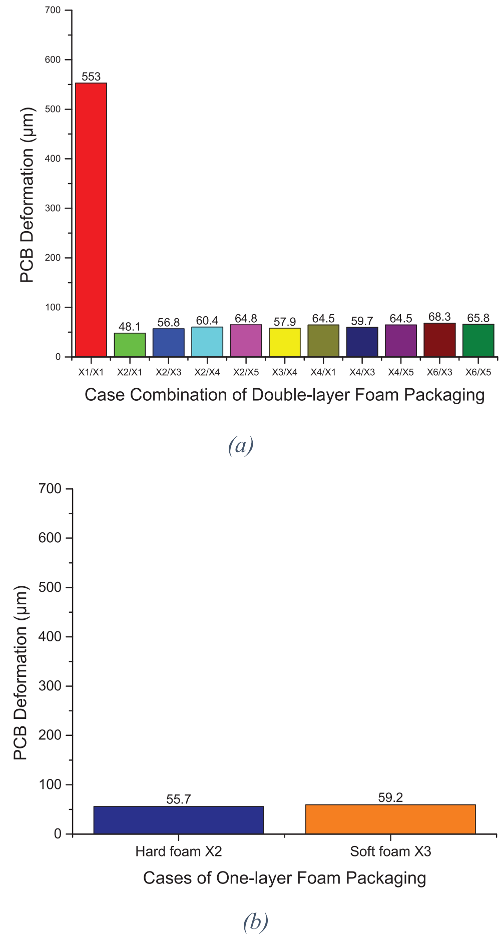


Fig. 10. Maximum out-of-plane deformation of PCB for different cases. (a) Simulation results of double-layer foam packaging. (b) Simulation results of one-layer foam packaging.

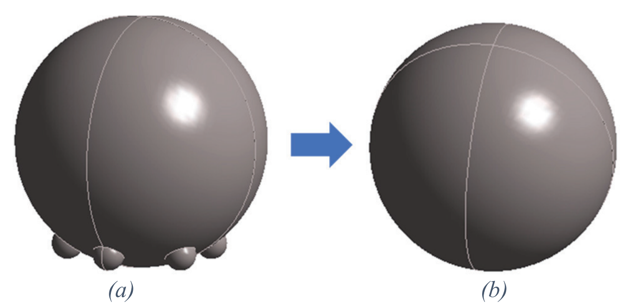


Fig. 11. 3-D model comparison between outer pimple texture and bare/plain outer texture. (a) Outer pimple texture. (b) Bared/plain outer texture.

Fig. 11. Fig. 11(a) illustrates the pimple design for the foam packaging. To optimize computational efficiency, only the bottom pimple texture was modeled, as the bottom pimples are the primary contributors to shock energy reduction during bottom drop impacts, while the other pimples have negligible impact on shock mitigation. Fig. 11(b) displays the bare outer texture, which eliminates the pimple texture, thereby reducing manufacturing costs and saving volume. The simulation results are summarized in Table III. The deformation of the PCB for the pimple-textured cases was only marginally lower than that of the bare-textured cases. As a result, the outer pimple texture was deemed unnecessary for this design, offering the potential

TABLE III
SIMULATION RESULTS OF THE STUDY EFFECT OF OUTER TEXTURE STRUCTURE

| PCB Deformation | | |
|---|---|---|
| PCB Thickness | With outer texture | Without outer texture |
| 125 mil | 51.9 µm | 58 µm |
| 93 mil | 60.3 µm | 65.8 µm |
| 65 mil | 61.1 µm | 73.5 µm |

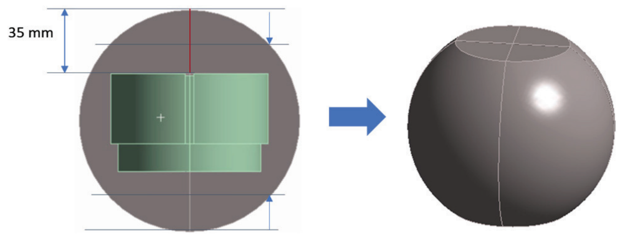


Fig. 12. 3-D model for foam packaging cutoff cases.

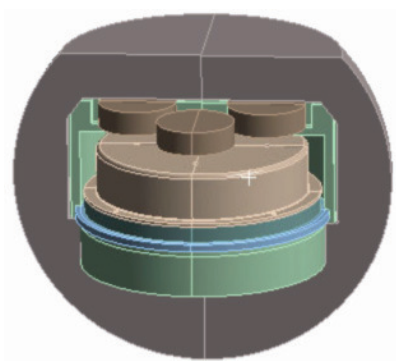

Fig. 13. 3-D model of Acron foam packaging shape design.

TABLE IV
SIMULATION RESULTS OF THE STUDY EFFECT OF PACKAGING VOLUME

| Case | Volume | PCB Deformation |
|---|---|---|
| Cut off 0 mm | 754 $cm^3$ | 53.1 µm |
| Cut off 10 mm | 724 $cm^3$ | 60.8 µm |
| Cut off 20 mm | 625 $cm^3$ | 81.7 µm |

for reduced material usage and manufacturing complexity without compromising performance.

To reduce the overall volume of the device, the spherical packaging model was truncated at the top and bottom at different distances—specifically 10 and 20 mm—given that the total thickness of the spherical packing is 35 mm, as shown in Fig. 12. The simulation results for these modifications are summarized in Table IV. The data in Table IV indicate that the 10-mm cutoff is an acceptable solution. This is because the deformation of the PCB remains within a tolerable range, while still achieving a reduction in volume. Additionally, after evaluating the full model, it was found that the center of gravity is located above the central electrode. This means that a 10-mm reduction in spherical packing on the battery side is feasible, while the other side can retain its spherical structure, resulting in what is referred to as the "Acorn structure" (illustrated in Fig. 13).

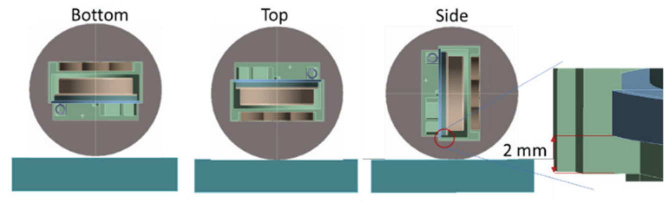


Fig. 14. Different drop directions of sphere foam packaging design.

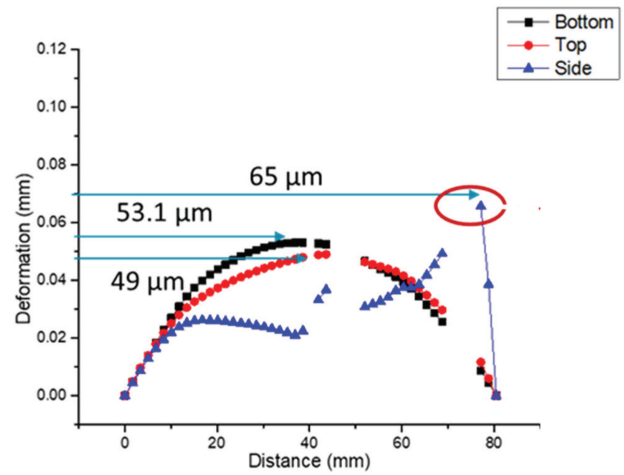


(a)

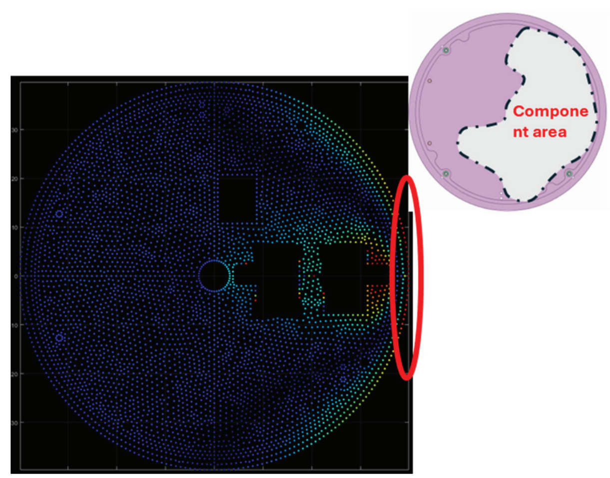


(b)

Fig. 15. Maximum out-of-plane deformation of PCB along the path in different drop directions. (a) PCB out-of-plane deformation for different drop orientations. (b) Warpage contour plot of side drop to indicate the maximum deformation location.

## F. Different Drop Directions

After verifying various designs, simulations were conducted to assess the performance of the design under different drop directions, ensuring its suitability for impacts from various orientations. The foam structure utilized in these simulations consists of a single hard foam layer with spherical packaging, as shown in Fig. 14. For the side drop scenario, since PCB side edge would impact to the ground and the location of center gravity is above PCB, which means the bending force would concentrate on PCB edge area, modifications were made to the battery holder by extending its sidewall height to envelop the side of the PCB, as also depicted in Fig. 14. This adjustment helps mitigate the significant deformation kink observed in the PCB during side impacts. As shown in Fig. 15, the maximum out-of-plane deformation of PCB deformation in all three drop directions is less than 100 $\mu$m. Although a pronounced kink is visible in the curve for the side drop, the PCB deformation contour in Fig. 15 reveals that this kink occurs at the interface between the battery holder and the PCB, an area without any components. Therefore, this localized max out-of-plane deformation does not affect the integrity of the components, and the overall design is deemed to meet the performance targets at this stage.

## IV. Conclusion

This study addressed several critical design aspects to optimize PCB performance under impact conditions. First, the incorporation of the bottom stiffener significantly reduced out-of-plane deformation of PCB, enhancing its rigidity during impact. Second, the re-evaluation of the outer texture and foam packaging design showed that, even without previous design features, PCB deformation remained comparable, suggesting these elements may not be essential. Third, adjustments to the foam packaging structure were made to reduce volume without compromising PCB deformation, offering benefits from both manufacturing and cost perspectives. Lastly, drop impact simulations across multiple orientations demonstrated that the overall structural design is robust and performs effectively under various impact scenarios.

## References


[1] G. Refai-Ahmed et al., "Qualification of high coplanarity package for general purpose processor," in *Proc. IEEE 25th Electron. Packag. Technol. Conf. (EPTC)*, Dec. 2023, pp. 834–841, doi: 10.1109/EPTC59621.2023.10457671.

[2] Y. Lai, P. Yin, J. Yang, J. Ha, K. A. Deo, and S. Park, "Reflow oven zone temperature advisor using the AI-driven smart recipe generator," in *Proc. IEEE 73rd Electron. Compon. Technol. Conf. (ECTC)*, May 2023, pp. 1773–1778.

[3] Y. Lai et al., "The optimal solution of reflow oven recipe based on physics-guided machine learning model," in *Proc. 21st IEEE Intersociety Conf. Thermal Thermomechanical Phenomena Electron. Syst. (iTherm)*, May 2022, pp. 1–6.

[4] Y. Lai et al., "A deep learning approach for reflow profile prediction," in *Proc. IEEE 72nd Electron. Compon. Technol. Conf. (ECTC)*, May 2022, pp. 2269–2274.

[5] Y. Lai, K. Pan, C. Cai, P. Yin, J. Yang, and S. Park, "Smarter temperature setup for reflow oven to minimize temperature variation among components," *IEEE Trans. Compon., Packag., Manuf. Technol.*, vol. 12, no. 3, pp. 562–569, Mar. 2022.

[6] Y. Lai, J. H. Ha, K. A. Deo, J. Yang, P. Yin, and S. Park, "Reflow recipe establishment based on CFD-informed machine learning model," *IEEE Trans. Compon., Packag., Manuf. Technol.*, vol. 13, no. 1, pp. 127–134, Jan. 2023.

[7] J. Ha, J. Yang, P. Yin, K. A. Deo, C. Cai, and S. Park, "Investigation on fatigue life of non-symmetric solder joints in chip resistors," in *Proc. IEEE 73rd Electron. Compon. Technol. Conf. (ECTC)*, vol. 86557, May 2023, pp. 840–845.

[8] J. Ha, Y. Lai, J. Yang, P. Yin, and S. Park, "Effect of differently shaped solder joints of chip resistor on fatigue life," *J. Electron. Packag.*, vol. 146, no. 2, Jun. 2024, Paper EP-23-1033.

[9] J. Ha et al., "Shape dependency of fatigue life in solder joints of chip resistors," in *Proc. IEEE 72nd Electron. Compon. Technol. Conf. (ECTC)*, May 2022, pp. 1489–1494.

[10] W. Oh, N.-C. Park, Y.-P. Park, and S. Yoo, "Analysis and improvement of shock performance of a container for the cartridge in a Blu-ray type archiving system," *Microsyst. Technol.*, vol. 21, no. 12, pp. 2629–2640, Dec. 2015.

[11] M.-C. Pan and P.-C. Chen, "Drop simulation/experimental verification and shock resistance improvement of TFT-LCD monitors," *Microelectron. Rel.*, vol. 47, no. 12, pp. 2249–2259, Dec. 2007.

[12] F. M. Shuaeib, A. M. S. Hamouda, S. V. Wong, R. S. R. Umar, and M. M. Ahmed, "A new motorcycle helmet liner material: The finite element simulation and design of experiment optimization," *Mater. Des.*, vol. 28, no. 1, pp. 182–195, Jan. 2007.

[13] C. Fremgen, L. Mkrtchyan, U. Huber, and M. Maier, "Modeling and testing of energy absorbing lightweight materials and structures for automotive applications," *Sci. Technol. Adv. Mater.*, vol. 6, no. 8, pp. 883–888, Jan. 2005.

[14] K. E. Jackson, M. S. Annett, E. L. Fasanella, and M. A. Polanco, "Material model evaluation of a composite honeycomb energy absorber," in *Proc. 12th Int. LS-DYNA Users Conf.*, no. NF1676L-13754, 2012.

[15] D. Yu, J. B. Kwak, S. Park, S. Chung, and J.-Y. Yoon, "Effect of shield-can design on dynamic responses of PCB under board level drop impact," in *Proc. Electron. Photon.*, Jan. 2009, pp. 305–310.

[16] P. Yin, S. Park, and G. Pandiarajan, "Shipping container design improvement analysis for drop/shock loading," in *Proc. IEEE 71st Electron. Compon. Technol. Conf. (ECTC)*, Jun. 2021, pp. 2145–2150.

[17] D. Yu, J. B. Kwak, S. Park, and J. Lee, "Dynamic responses of PCB under product-level free drop impact," *Microelectron. Rel.*, vol. 50, no. 7, pp. 1028–1038, Jul. 2010.

[18] P. Yin, H. Wang, J. Xu, V. Pham, and S. Park, "Shock performance enhancement of a container for rack server," in *Proc. 19th IEEE Intersociety Conf. Thermal Thermomech. Phenomena Electron. Syst. (ITherm)*, Jul. 2020, pp. 1264–1270.

[19] P. Yin, "Drop-impact simulation and validation of foam packaging," ProQuest Dissertations & Theses, Binghamton Univ., Binghamton, NY, USA, 2020.

[20] U. E. Ozturk and G. Anlas, "Finite element analysis of expanded polystyrene foam under multiple compressive loading and unloading," *Mater. Des.*, vol. 32, no. 2, pp. 773–780, 2011.

[21] B. Sambamoorthy and T. Halder, "Characterization and component level correlation of energy absorbing (EA) polyurethane foams (PU) using LS-DYNA material models," in *Proc. 3rd Eur. LS-DYNA Conf.* France: CRIL Technol., 2001, p. 8.

[22] P. Yin, S. Park, B. Jacob, L. Yin, and A. Gowda, "Package design through reliable predictive modeling and its validation," in *Proc. IEEE 72nd Electron. Compon. Technol. Conf. (ECTC)*, May 2022, pp. 1738–1744.